02

Excitation mechanism of pulsed cathodoluminescence of cerium in yttrium-aluminum garnet

© V.I. Solomonov, V.V. Lisenkov, A.V. Spirina, A.S. Makarova

Institute of Electrophysics, Ural Branch, Russian Academy of Sciences, Yekaterinburg, Russia

e-mail: plasma@iep.uran.ru

Received December 25, 2024
Revised November 25122024
Accepted February 06, 2025

The pulsed cathodoluminescence of a cerium ion in ceramic samples of yttrium-aluminum garnet with a ceria content of 0.1, 0.5, 1.0, 2.0, 3.0, 4.0, and 5.0 at.% was studied. These samples were irradiated in air at room temperature with a 2 ns-duration electron beam with an average electron energy of 170 keV and a current density of 130 A/cm^2. It enables to simulate the external ionizing radiation for scintillators. Two broad luminescence bands were observed at 570 nm and at 350 nm, being the results of the Ce^{3+} ion d-f transition and the recombination of a self-trapped exciton, respectively. The cerium luminescence band center shifts to the long-wavelength region with an increase in the content of ceria. It is found that the intensity decay of the cerium band, measured for each concentration at a wavelength of 570 nm, is characterized by two maxima in the nanosecond ($t_{m1} \approx 3$ ns) and microsecond ($t_{m2} \approx 1.3\,\mu$s) time intervals. The first maximum is shown to be formed due to, firstly, the excitation of Ce^{3+} *d*-levels by secondary electrons generated by beam electrons and, secondly, spontaneous emission with a characteristic time of $\tau_s = 100 \pm 10$ ns. The second maximum arises when the excited Ce^{3+} is formed during the recombination of Ce^{2+} and Ce^{4+} ions produced by the electron beam. After the second maximum, the intensity decay of the band is described by a hyperbolic law with a characteristic time of $30-75\,\mu$s, depending on the content of cerium ions, and the light sum of this recombination luminescence is 60% of the total luminescence light sum of the band. The luminescence intensity decay of the band at 350 nm is monotonic and a characteristic decay time is 63.7 ns for a sample with a ceria content of 0.1 at.% and about 10.5 ns for samples with a ceria content of 0.5–5 at.%.

Keywords: pulsed cathodoluminescence, cerium, yttrium-aluminum garnet, kinetics, rise, decay, characteristic times.

DOI: 10.61011/EOS.2025.02.61020.6934-24

Introduction

Yttrium-aluminum garnet activated by cerium ions (Ce:YAG) is used as a detector of X-ray and soft gamma radiation due to its scintillation properties [1–3]. To date, various methods of manufacturing such scintillators in the form of single crystals have been developed, for example, by „Azimuth photonics“ (https: azimp.ru) and JSC „LLS“ St. Petersburg, as well as optically transparent ceramics Ce:YAG by „Metalaser“ (ru.metalaser.com). These scintillators emit in a wide band of ion Ce^{3+} centered at $\lambda \approx 550-560$ nm with a decay time of 60–70 ns. At the same time, the presence of a second slower component with 260 ns is noted in the luminescence decay („Metalaser“ data). The characteristics of the luminescence intensity decay measured at a wavelength of 545 nm in Ce:YAG ceramic scintillators excited by 15 ns-duration electron beam with an average electron energy of 150 keV are provided in Ref. [4]. This study confirmed that the decay is well approximated by the sum of two exponentials with characteristic times differing several times, but with a steady decreasing trend of both characteristic times from 110 to 26 ns and from 562 to 338 ns with an increase of the content of cerium ions from 0.1 to 5 at.%. It is also shown in Ref. [4] that, at a cerium content of 1 at.% in YAG, the relative light yield scintillations is 32% of the reference CsI-Tl scintillator, but the reasons for the relatively low light yield are not discussed. However, the overview article [5] reports that the scintillation yield critically depends on the presence (concentration) of electron traps leading to a change in time characteristics.

This paper is devoted to the study of the pulsed cathodoluminescence (PCL) decay kinetics of cerium ions in Ce:YAG ceramic samples excited by 2 ns-duration electron beam for identifying the mechanisms of excitation and quenching of luminescence, as well as to clarify the scintillation capabilities of these ceramic substances.

Samples and experimental equipment

Nanopowders of Al_2O_3 and Ce:Y_2O_3 were obtained from raw materials (Al_2O_3, Y_2O_3, and CeO_2 micropowders) with a purity of 99.99% using the laser ablation method. These nanopowders were mixed in garnet stoichiometry taking

into account the production of ceramics with the cerium content indicated below.

Samples of transparent Ce:YAG ceramics in the form of polished discs with a diameter of 10–12 mm and a thickness of 2.2 mm containing 0.1, 0.5, 1, 2, 3, 4 and 5 at.% of cerium oxide were studied. They were produced by the Institute of Electrophysics of the Ural Branch of the Russian Academy of Sciences using the method described in Ref. [6,7]. Structurally, the samples were densely packed cubic phase crystallites with an average size varying from 11 to 6 μm with increasing cerium content. X-ray phase analysis performed using D8 Discover diffractometer showed that all samples were single-phase and represented the structure of yttrium-aluminum garnet ($a = 12.017(3)$ Å, coherent scattering region ≈ 500 nm, $\rho = 4.546(4)$ g/cm^3).

Luminescent measurements were carried out in air at room temperature. The source of PCL excitation was an electron beam with a FWHM duration of 2 ns with an average electron energy of 170 keV with a current density of 130 A/cm^2, which was formed in the vacuum diode of the CLAVI setup [8]. Such an electron beam is a fine model of ionizing radiation for scintillators. The overview luminescence spectrum in the range from 200 to 850 nm was recorded by transmitting the luminescence flux from the sample via a multicore quartz light guide into two OS-13 polychromators with time-integrating CCD photodetectors with sensitivity in the range of 200–450 and 400–850 nm, respectively. The spectra were combined at a wavelength of 400 nm. The intensities of the luminescence bands recorded by these photodetectors were not adjusted among themselves. The wavelength measurement error was 0.5 nm.

To assess the optical quality of ceramic samples, their light transmission was measured in the range from 200 to 1100 nm using a Shimatzu UV-1700 spectrophotometer.

The kinetics of individual luminescence bands was measured using modernized CLAVI setup, a detailed description of which is provided in Ref. [9]. The luminescence flux in this setup was output to the MDR-41 monochromator that was used to isolate a certain section of the luminescence band of intrinsic defect and cerium ions with a width of 1.5 and 3 nm, respectively. A FEU-100 photomultiplier tube (PMT), operating in a nonlinear current mode, was used as a receiver [10]. The signal from the PMT via a coaxial cable was applied to the input resistance $R = 1$ MΩ of a Keysight DSOX2014A oscilloscope. In this case, the photocurrent I_p was determined via the measured voltage drop across the input resistance of the oscilloscope U_R as follows:

$$RI_p = LC\frac{d^2U_R}{dt^2} + RC\frac{dU_R}{dt} + U_R. \qquad (1)$$

Here L and C are the inductance and the capacitance of the PMT measuring circuit. It was believed that the photocurrent is proportional to the current intensity of the measured luminescence band.

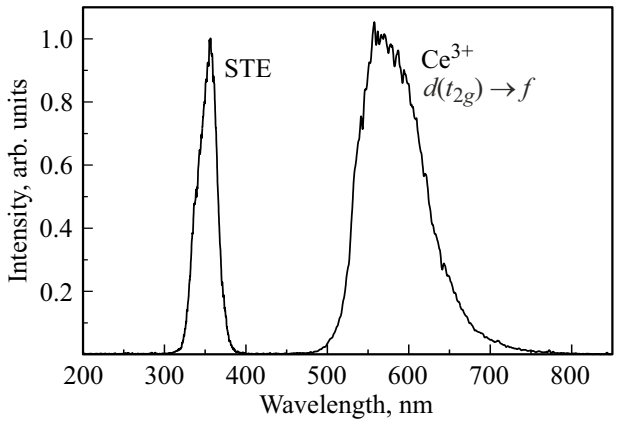

Figure 1. The PCL spectrum of the Ce:YAG ceramic sample with a cerium oxide content of 1 at.%. For clarity, the bands of intrinsic luminescence and cerium luminescence are normalized by one.

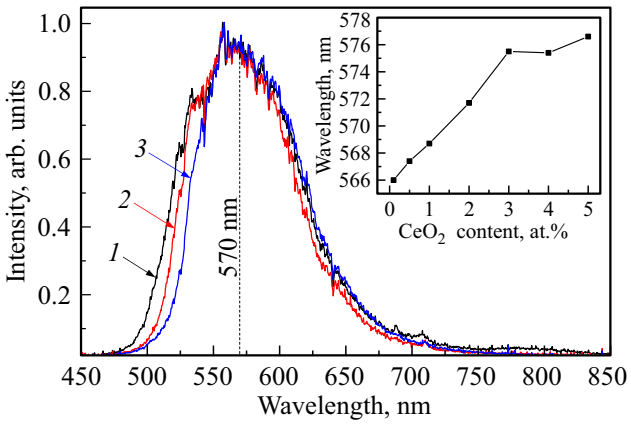

Figure 2. PCL spectra of Ce:YAG ceramic samples with a cerium oxide content of 0.1 (curve *1*), 0.5 (curve *2*) and 3 at.% (curve *3*). For clarity, the intensity maxima of the bands are reduced to the same value. The inset shows the dependence of the wavelength of the band center on the cerium oxide content in the samples.

Results and their discussions

The PCL spectra of all the studied samples turned out to be qualitatively similar. The PCL spectrum of a ceramic Ce:YAG sample with a cerium oxide content of 1 at.% is shown in Fig. 1 for illustration. It shows two strong wide bands with centers at $\lambda \approx 350$ and 570 nm. The ultraviolet band at 350 nm is a intrinsic luminescence band associated with the recombination of a self-trapped exciton (STE) [11]. It is more than an order of magnitude weaker than the band at 570 nm. The intensity of the intrinsic luminescence band monotonously decreases as the cerium oxide content in the samples increases from 0.5 to 5 at.%.

Fig. 2 shows the behavior of the yellow band at 570 nm in the PCL spectra of Ce:YAG ceramic samples with a cerium oxide content of 0.1, 0.5, and 3 at.%. This band is described with a correlation coefficient of more than 98% by the Gaussian function, from which such band parameters

as width and maximum position have been determined. As the cerium oxide content in the samples increases, the wavelength of the center of this band shifts to the long-wavelength side (Fig. 2, inset), and its FWHM does not change within the measurement error and is 75 nm. The exception is a sample with a cerium oxide content of 0.1 at.%, for which this value is 83 nm. The reason for this is not entirely clear. It is possible that the narrowing of the bands is attributable to concentration quenching when the cerium oxide content is greater than 0.1 at.%. This band is associated in Ref. [4,11–13] with the emission of the Ce^{3+} ion at the $d-f$-transition. The kinetics of luminescence was recorded at a wavelength of 570 nm. This is approximately the average value between the maximum and minimum wavelength values of the band center, which varies depending on the concentration of cerium.

The ion Ce^{3+} replaces the main Y^{3+} cation in the dodecahedral position. d-levels of cerium ion are split in this position into an orbital doublet e_g (upper) and a triplet t_{2g} (lower), between which the energy distance is equal to the strength of the crystal field in the dodecahedral position YAG, $\Delta \approx 17000\,\mathrm{cm}^{-1}$ [14]. The absorption spectra [4] of these Ce:YAG ceramic samples have two strong bands at $\lambda = 337$ and 457 nm and two weaker bands at $\lambda = 258$ and 301 nm. The difference of the wave numbers $\Delta\nu = 16880\,\mathrm{cm}^{-1}$ between the bands at $\lambda = 457$ and 258 nm corresponds closely to the strength of the crystal field Δ. Therefore, these two bands can be associated with the absorption to the e_g and t_{2g} Stark levels of the Ce^{3+} ion. The remaining two absorption bands at $\lambda = 301$ and 337 nm, as in Ref. [13], should be attributed to absorption by other defects. Therefore, the strong yellow band observed in the PCL spectrum (Fig. 1) should be considered the result of $d(t_{2g}) \rightarrow f$-transition in Ce^{3+} ions. For it, the Stokes shift relative to the absorption band is about $4025\,\mathrm{cm}^{-1}$. Radiation from the e_g-components of the d-level to the ground state of Ce^{3+} ion is not explicitly manifested. Taking into account the above Stokes shift, the emission band at the transition from this level should appear in the region of 288 nm.

For all yttrium-aluminum garnet samples, the behavior of U_R (1) of both PCL bands has an extreme appearance (Fig. 3). Moreover, the area before reaching the maximum has a monotonously increasing character for the intrinsic band at 350 nm (Fig. 3, inset, curve *1*), while a plateau is observed in the range of $0.4-4\,\mu$s in the kinetic curve of the cerium band at 570 nm of all samples (Fig. 3, inset, curve *2*).

The equation (1) using U_R oscillograms of different time resolution was resolved using MathCad. Noise filtering was performed using the fast Fourier transform function.

The reconstructed kinetic curves of the photocurrent I_p from the corresponding luminescence bands turned out to be qualitatively similar for all ceramic samples. However, the kinetic curves of the cerium ion band and its intrinsic band significally differ from each other. The behavior of the band intensities at 350 and 570 nm on a logarithmic scale for a sample with a cerium oxide content of 3 at.% is shown in Fig. 4 as an illustration. It was assumed that the photocurrent I_p is proportional to the current intensity I of the measured luminescence band.

The approximation was performed in the range $0.01-2\,\mu$s for the intrinsic band at $\lambda = 350$ nm (Fig. 4, *a*), in which the kinetic curve has the form of a straight line with the smallest noise component on a logarithmic scale. The luminescence intensity curve $I(t)$ of this band is well described by the hyperbolic Becquerel law of the first degree:

$$I(t) = I_0\left(1 + \frac{t}{\tau_{tr}}\right)^{-1}, \qquad (2)$$

where I_0 is the luminescence intensity at the moment of termination of excitation, τ_{tr} is the characteristic time due to linear recombination of „free“ electrons and holes generated in matter by an electron beam at its intrinsic center. The characteristic luminescence decay time on the 350 nm spectral band for the studied samples is about 10.5 ns. The exception is a ceramic sample with a cerium oxide content of 0.1 at.%, which has $\tau_{tr} = 63.5$ ns.

The photocurrent curves of the cerium PCL band at $\lambda = 570$ nm of all samples have two intensity maxima and an inflection point in the vicinity of $t_{ip} \approx 1\,\mu$s (Fig. 4, *b*).

Mathematical models based on kinetic equations were used to determine the characteristic luminescence times of cerium and the mechanisms of its excitation. The luminescence intensity behavior over time $I(t)$ was approximated by numerically solving these kinetic equations for each studied sample. For convenience, the intensity $I(t)$ was calculated in a dimensionless form, and the constants included in the kinetic equations were selected based on the requirement of maximum similarity of the approximation with experimental data.

It is known that a beam of fast electrons ionizes matter, and the energy spectrum of secondary electrons extends over the entire width of the conduction band, including its

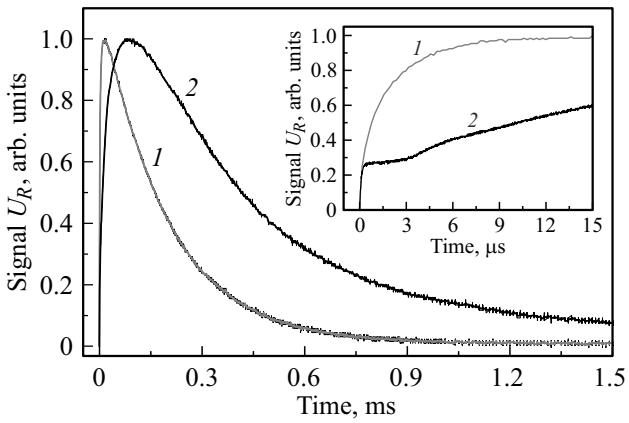

Figure 3. Normalized waveforms from the PMT (U_R) for bands at 350 (*1*) and 570 nm (*2*) of the Ce:YAG sample with a cerium oxide content of 3 at.%. The inset shows the initial sections of the waveforms of both bands.

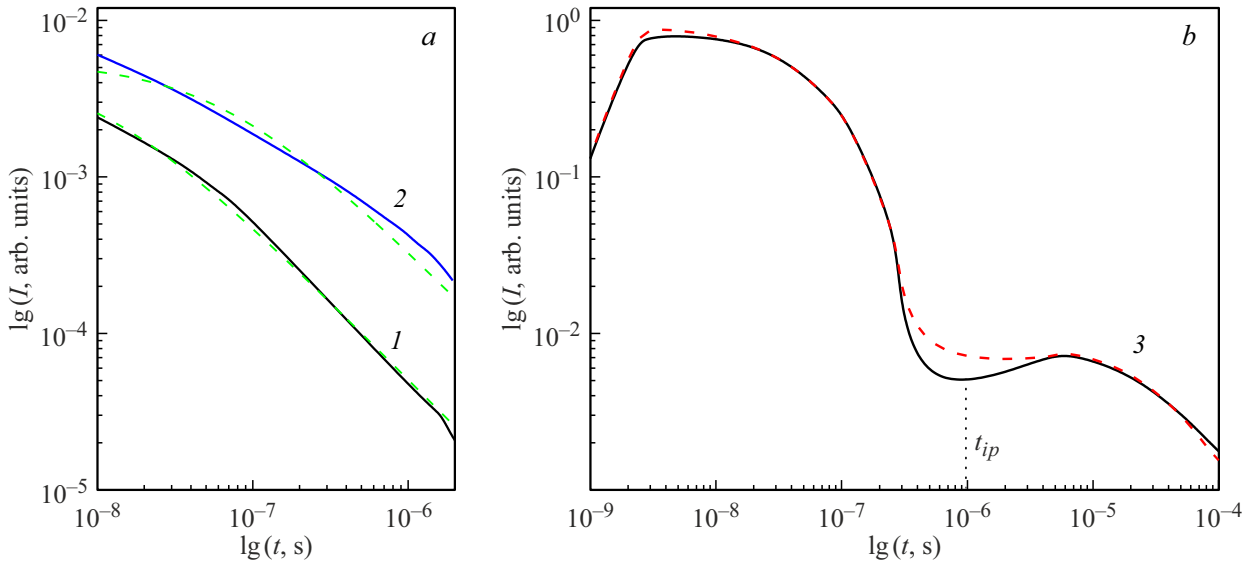

Figure 4. The intensity behavior of PCL bands at 350 (*a*) and 570 nm (*b*) in Ce:YAG ceramic samples with a cerium oxide content of 3 (curves *1, 3*) and 0.1 at.% (curve *2*), obtained as a result of solving equation (1). Green dashed line shows the approximation by a hyperbolic function (2), red dashed line shows the approximation according to the kinetic model for the PCL of cerium ions in YAG, presented in the text.

uppermost levels. The relaxation of electron energy with a characteristic time of the order of $\tau_{\text{rel}} \sim 10^{-12}$ s takes place in the processes of interaction with phonons, as well as with defects (including impurities) of the crystal lattice. In this case, the population of excited states of trivalent cerium ions with a concentration of $[Ce^{3+*}]$ in the short-range afterglow ($t \le t_{ip} \approx 1\,\mu$s) can be represented by the following set of equations:

$$\frac{dn_e^*}{dt} = \frac{N\sigma_i J_b(t)}{e} - \nu_{\text{rel}} n_e^*, \tag{3}$$

$$\frac{d[Ce^{3+*}]}{dt} = \eta_{n-\text{Ce}} \nu_{\text{rel}} n_e^*, \tag{4}$$

Here n_e^* is the concentration of secondary electrons with energy higher than $E_g + E_i$, where E_g is the band gap, and E_i is the excitation energy of the radiative level; $J_b(t) = J_{b0} \sin(\pi t/\tau_b)$ is an electron beam current density pulse, the form of which is represented as the first half-cycle of a sine wave with the pulse amplitude J_{b0} and a total duration of $\tau_b = 3$ ns [15]; N is the concentration of atoms in a ceramic sample; σ_i is the ionization cross section; e is the electron charge; $\eta_{n-\text{Ce}}$ is the fraction of the relaxing energy of secondary electrons transferred to the excitation of Ce^{3+} ions; $\nu_{\text{rel}} = 1/\tau_{\text{rel}}$. Since $\tau_{\text{rel}} \ll \tau_b$, the dependence of n_e^* on time will be determined by the form of the exciting electron beam, i.e. it can be described by the formula

$$n_e^*(t) = \frac{N\sigma_i J_{b0}}{e\nu_{\text{rel}}} \sin\left(\frac{\pi t}{\tau_b}\right). \tag{5}$$

Assuming that the luminescence intensity is proportional to $[Ce^{3+*}]$, the following kinetic equation for intensity can be used for the short-range afterglow of the band at $\lambda = 570$ nm:

$$\frac{dI}{dt} = \hbar\omega c \left(\frac{n_e^*(t)}{\tau_s} + \frac{\eta_d n_d}{\tau_l} \exp\left(-\frac{t}{\tau_l}\right)\right) - I\left(\frac{1}{\tau_s} + \frac{1}{2\sqrt{\tau_f t}}\right). \tag{6}$$

Here the first two right-hand terms, standing in the first brackets, describe the excitation of the radiative level: the first term describes the „direct“ excitation of the radiative level of cerium by fast secondary electrons, while the second term with the characteristic time τ_l describes its excitation by energy transfer from other defects. In this case, n_d is the concentration of excited defects, η_d is the part of the excitation energy transferred to excited Ce^{3+*} ions, $\hbar\omega$ is the photon energy, c is the speed of light. The third and fourth terms of the equation in the second brackets (6) describe the de-excitation of the radiative level in the processes of spontaneous emission and Förster quenching with the characteristic times of these processes τ_s and τ_f, respectively. The latter mechanism is the most common for intracenter luminescence in solids caused by nonradiative dipole-dipole energy transfer from the donor (Ce^{3+*}) to acceptors, which can be constituted by various lattice defects.

The equation (6) was solved numerically for each studied sample. The parameters of the excitation and quenching processes of the radiative level of cerium obtained as a result of the solution for all the studied samples are listed in Table 1. In the first column, the light transmission of the samples in the vicinity of the wavelength at 570 nm is shown in parentheses.

Table 1. Characteristic luminescence decay times of the Ce^{3+} band at 570 nm (t_s and t_f) and the ratio of excited process rate amplitudes (I_l/I_{b0}) in the short-range afterglow

Content of cerium oxide in sample, at.% (light transmission, %)	τ_s, ns	τ_f, ns	$\frac{I_l}{I_{b0}}$
0.1 (81.4)	100	12	$1.0 \cdot 10^{-2}$
0.5 (77.1)	97	6500	$< 10^{-4}$
0.5 (76.6)	100	6900	$< 10^{-4}$
1 (79.9)	110	346	$1.5 \cdot 10^{-3}$
2 (37.3)	103	11100	$< 10^{-4}$
3 (66.0)	110	309	$1.4 \cdot 10^{-3}$
4 (34.9)	100	28	$9.7 \cdot 10^{-3}$
5 (33.1)	90	25	$1.0 \cdot 10^{-2}$

It turned out that the second term of equation (6), which describes the transfer of energy to the cerium ion from defects in the crystal structure, is characterized by a time $\tau_l = 100$ ns with a spread in values of 20 ns for samples with different cerium contents. The amplitudes of this process I_l (as well as the ratio of amplitudes I_l/I_{b0}) have significantly different values and do not correlate either with the cerium content in the samples or with their light transmission. This fact and the absence of a dependence of τ_l on the concentration of Ce^{3+} ions suggest that there are no cerium ions in the defects involved in this process. The integral contribution to the excitation of the radiative level of cerium by energy transfer from these defects $I_l\tau_l$ is less than the contribution from „direct" excitation by secondary electrons $I_{b0}\tau_b$. The ratio of these contributions reaches a value of 1/3 only for samples with a cerium content of 0.1, 4, and 5 at.%. Therefore, the excitation mechanism of the cerium radiative level, described by the second term of equation (6) cannot be neglected for these samples, and the mechanism and nature of defects capable of transferring energy to the radiative level of the cerium ion require additional investigation.

The characteristic spontaneous emission time $\tau_s \approx 100$ ns within 10% turned out to be the same for all samples. This proves that it is a coefficient of the radiative level. The decrease of intensity after the first maximum is determined not only by this time, but also by the Förster quenching time of the radiation level τ_f:

$$I(t) \sim \exp\left\{-\frac{t}{\tau_s} - \left(\frac{t}{\tau_f}\right)^{1/2}\right\}. \quad (7)$$

Table 1 shows that the Förster times τ_f differ significantly from one sample to another, and this time does not correlate with the light transmission of the samples. However, for samples with a high Förster quenching rate, there is an increased ratio of I_l/I_{b0} and a distinct inverse correlation between τ_f and the ratio of I_l/I_{b0}. This means that some of the defects active in the Förster quenching of the cerium radiative level transfer their energy to the radiative level with a characteristic time of τ_l. The law of decay (7) was essentially approximated in [4] by the sum of two exponentials. As a result, two effective intensity decay times were obtained, depending on the concentration of cerium in the samples.

The dominant excitation mechanism of the radiative level changes in the long-range afterglow ($t > t_{ip} \approx 1\,\mu$s). Earlier, when studying the kinetics of „free" (secondary) electrons and holes generated in matter by an electron beam, it was shown in Ref. [16] that for a time longer than the characteristic linear recombination time of these charge carriers, linear recombination becomes the dominant mechanism of their concentration decrease. It occurs in the processes of localization of secondary electrons and holes on defects in the crystal structure, and the decrease of their concentrations proceeds exponentially with characteristic times t_{p1} and t_{p2}. We assume that the cerium ions are the main traps since it has stable valences of II, III, IV. That is, when impurity Ce^{3+} ions capture „free" electrons, a filled trap is briefly formed — Ce^{2+} ion, and when a hole is captured — Ce^{4+} ion. The possibility of the existence of Ce^{2+} ion is shown in Ref. [17].

The recombination of these ions

$$Ce^{2+} + Ce^{4+} \rightarrow Ce^{3+} + Ce^{3+*} \quad (8)$$

is believed to lead to the formation of an excited Ce^{3+*} ion and is accompanied by luminescence in the microsecond range. It is assumed that such capturing ensures equal concentrations of divalent $[Ce^{2+}]$ and tetravalent $[Ce^{4+}]$ cerium ions at each time point. In this case, the simplest set of equations has the following form for describing the kinetics of the long-range afterglow

$$\frac{d[Ce^{2+}]}{dt} = \frac{d[Ce^{4+}]}{dt} = A_{p1}\exp\left(-\frac{t}{\tau_{p1}}\right) + A_{p2}\exp\left(-\frac{t}{\tau_{p2}}\right) - \beta_r[Ce^{2+}][Ce^{4+}], \quad (9)$$

$$\frac{d[Ce^{3+*}]}{dt} = \beta_r[Ce^{2+}][Ce^{4+}] - [Ce^{3+*}]\left(\frac{1}{\tau_s} + \frac{1}{2\sqrt{\tau_f t}}\right), \quad (10)$$

where A_{p1} and A_{p2} are amplitudes of localization processes of „free" electrons and holes on impurity Ce^{3+} ions, β_r is the recombination coefficient of Ce^{2+} and Ce^{4+} ions. In this case, the radiation intensity is equal to

$$I = \frac{\lfloor Ce^{3+*} \rfloor}{\tau_s} h\nu. \quad (11)$$

Since the proportionality coefficient between the emission intensity and the PMT photocurrent is unknown, it is also more convenient to solve this set of equations in a dimensionless form. Calculations based on experimental long-range afterglow waveforms have shown that the characteristic times $\tau_{p1} = 7.0$ ns and $\tau_{p2} = 3.5$ ns are the same for all samples. This indicates that the linear recombination of

Table 2. The kinetics parameters of the long-range afterglow of the Ce^{3+} band at 570 nm

Content of cerium oxide in the sample, at.%	$\frac{A_{p2}}{A_{p1}}$	Recombination time $(\beta_r n_0)^{-1}$, μs
0.1	0.11	38.8
0.5	0.15	74.1
1.0	0.40	64.2
2.0	0.35	67.2
3.0	0.26	70.8
4.0	0.42	47.9
5.0	0.11	36.0

electrons and holes on crystal defects proceeds at different rates, and the role of impurity Ce^{3+} ions as such defects is small. Calculations also allow determining the characteristic times of quadratic recombination of cerium ions that have captured electrons and holes, $(\beta_r n_0)^{-1}$ (n_0 is the initial ion concentration), and the amplitude ratios A_{p2}/A_{p1} of localization processes of „free" electrons and holes on Ce^{3+} ions. The results of these calculations are provided in Table 2.

Table 2 shows that the amplitude A_{p1} of the charge localization process with a characteristic time $\tau_{p1} = 7$ ns in all cases is greater than the amplitude A_{p2} of the process with a time $\tau_{p2} = 3.5$ ns. At the same time, there is a correlation between an increase of the effect of the second process and an increase of the cerium content in the samples, with the exception of a sample with a cerium oxide content of 5 at.%. The characteristic recombination time, which determines the long-term decay of luminescence, tends to decrease with increasing concentration of cerium ions, especially pronounced for cerium contents from 3 to 5 at.%. It should be noted that the rise of luminescence under the action of this excitation mechanism slows down the intensity decay after the first maximum (Fig. 4, *b*).

The fractions of light sums of the short (nanosecond $0-1\,\mu$s) and long (microsecond $1-80\,\mu$s) luminescence ranges in the band at 570 nm were estimated by integrating kinetic curves (Fig. 4, *b*). They make up approximately 0.4 and 0.6 of the total light sum, respectively. Thus, more than half of the total light sum of the intracenter luminescence of the cerium ion occurs at the long-range (microsecond) stage of decay in the studied Ce:YAG samples, which is the reason for the small fraction of the scintillation response in the nanosecond range.

Conclusion

The decay kinetics of the intrinsic luminescence band at 350 nm is described by a hyperbolic law with a characteristic time of 63.7 ns for a sample with a cerium oxide content of 0.1 at.% and 10.5 ns for samples with a cerium oxide content of 0.5–5 at.%. This time is attributable to the linear recombination of „free" electrons and holes generated in matter by an electron beam.

In the kinetics of the pulsed cathodoluminescence band at 570 nm of the Ce^{3+} ion $d-f$ transition in yttrium-aluminum garnet, in addition to the intensity maximum in the nanosecond time range with a fast decay, the second intensity maximum at $1.3\,\mu$s was found. After this time point the intensity decay proceeds according to a hyperbolic law with a characteristic time of about $30-75\,\mu$s depending on the cerium content. It is shown that at the initial stage, coinciding in time with the duration of the electron beam, the excitation of the radiative level of cerium occurs as a result of relaxation of the energy of fast secondary electrons. At the second stage, the dominant mechanism of excitation of the radiative level is the recombination of ions Ce^{2+} and Ce^{4+}, formed as a result of the localization of slow free electrons and holes on Ce^{3+} ions, resulting in a second intensity maximum. Its value is approximately two orders of magnitude less than the first one, while the intensity decay time after the first maximum is approximately two orders of magnitude less than after the second one. As a result, the fraction of the light sums of the short and long time ranges of luminescence is 0.4 and 0.6 of the total light sum, respectively. This is the reason for the relatively low light yield of Ce:YAG scintillations in the nanosecond range.

Funding

This work is supported by the Ministry of Science and Higher Education of the Russian Federation, project № 124022200004-5.

Conflict of interest

The authors declare that they have no conflict of interest.

References

[1] K.J. Wilson, R. Alabd, M. Abolhasan, M. Safavi-Naeini, D.R. Franklin. Sci. Rep., **10** (1), 1409 (2020). DOI: 10.1038/s41598-020-58208-y
[2] A.A. Fyodorov, V.B. Pavlenko, M.V. Korzhik, W.P. Trower, R.F. Zuevesky. Radiat. Meas., **26** (2), 215 (1996). DOI: 10.1016/1350-4487(95)00293-6
[3] A. Ikesue. Ceram. Soc. Jpn., **108** (1263), 1020 (2000). DOI: 10.2109/jcersj.108.1263_1020
[4] V.V. Osipov, A.V. Ishchenko, V.A. Shitov, R.N. Maksimov, K.E. Lukyashin, V.V. Platonov, A.N. Orlov, S.N. Osipov, V.V. Yagodin, L.V. Viktorov, B.V. Shulgin. Opt. Mat., **71**, 98 (2017). DOI: 10.1016/j.optmat.2016.05.016
[5] M. Nikl, V.V. Laguta, A. Vedda. Phys. Stat. Sol. B, **245** (9), 1701 (2008). DOI: 10.1002/pssb.200844039
[6] S.N. Bagayev, V.V. Osipov, S.M. Vatnik, V.A. Shitov, I.Sh. Shteinberg, I.A. Vedin, P.F. Kurbatov, K.E. Luk'yashin, R.N. Maksimov, V.I. Solomonov, P.E. Tverdokhleb. Quantum Electron., **45** (5), 492 (2015). DOI: 10.1070/QE2015v045n05ABEH015769

[7] S.N. Bagayev, V.V. Osipov, E.V. Pestryakov, V.I. Solomonov, V.A. Shitov, R.N. Maksimov, A.N. Orlov, V.V. Petrov. J. Appl. Mech. and Techn. Phys., **56** (1), 150 (2015). DOI: 10.1134/S0021894415010228
[8] V.I. Solomonov, S.G. Michailov, A.I. Lipchak, V.V. Osipov, V.G. Shpak, S.A. Shunailov, M.I. Yalandin, M.R. Ulmaskulov. Laser Physics, **16**, 126 (2006). DOI: 10.1134/S1054660X06010117
[9] V.I. Solomonov, A.V. Spirina, A.S. Makarova. Phys. Solid State, **64** (13), 2088 (2022). DOI: 10.21883/PSS.2022.13.52306.24s
[10] V. Solomonov, A. Spirina, A. Makarova, A. Lipchak, A. Spirin, V. Lisenkov. J. Opt. Technol., **89** (12), 728 (2022). DOI: 10.1364/JOT.89.000728
[11] V.I. Solomonov, V.V. Osipov, V.A. Shitov, K.E. Luk'yashin, A.S. Bubnova. Opt. Spectrosc., **128** (1), 5 (2020). DOI: 10.1134/S0030400X20010221
[12] B. Sun, L. Zhang, T. Zhou, C. Shao, L. Zhang, Y. Ma, Q. Yao, Z. Jiang, F.A. Selim, H. Chen. J. Mater. Chem. C, **7**, 4057 (2019). DOI: 10.1039/C8TC06600K
[13] E.F. Polisadova, Tao Han, V.I. Oleshko, D.T. Valiev, V.A. Vaganov, C. Zhanga, A.G. Burachenko. Fund. Research, **12** (1), 103 (2017). DOI: 10.17513/fr.41987
[14] D.T. Sviridov, R.K. Sviridova, Yu.F. Smirnov. *Opticheskie spektry ionov perekhodnyh metallov v kristallah* (Nauka, M., 1976) (in Russian).
[15] S.N. Ivanov, V.V. Lisenkov. Tech. Phys., **55** (1), 53 (2010). DOI: 10.1134/S1063784210010093
[16] B.I. Solomonov, S.G. Mikhailov. *Impul'snaya katodolyuminescenciya i ee primenenie dlya analiza kondensirovannyh veshchestv* (UrO RAN, Ekaterinburg, 2003) (in Russian).
[17] R.Yu. Shendrick, A.S. Myasnikova, A.V. Egranov, E.A. Radzhabov. Opt. Spectrosc., **116** (5), 845 (2014). DOI: 10.1134/S0030400X14050221

Translated by A.Akhtyamov